Journal of Sound and Vibration 350 (2015) 73–90

Contents lists available at ScienceDirect

Journal of Sound and Vibration

journal homepage: www.elsevier.com/locate/jsvi

Thick hollow cylindrical waveguides: A theoretical, numerical and experimental study

Aleksandra Ziaja [a,b], Li Cheng [a,b,*], Zhongqing Su [a,b], Pawel Packo [c], Lukasz Pieczonka [c], Tadeusz Uhl [c], Wieslaw Staszewski [c]

[a] Department of Mechanical Engineering, The Hong Kong Polytechnic University, Hung Hom, Kowloon, Hong Kong
[b] The Hong Kong Polytechnic University Shenzhen Research Institute, Shenzhen 518057, China
[c] Department of Robotics and Mechatronics, AGH University of Science and Technology, Al. Mickiewicza 30, 30-059 Krakow, Poland

ARTICLE INFO

Article history:
Received 10 October 2014
Received in revised form
26 February 2015
Accepted 2 April 2015
Handling Editor: H. Ouyang
Available online 28 April 2015

ABSTRACT

The paper investigates elastic waves guided by thick-walled, hollow cylindrical structures. Theoretical, numerical and experimental investigations are presented to facilitate understanding of various wave propagation phenomena in thick-walled cylinders for potential damage detection applications. Semi-analytical analysis of dispersion characteristics is performed, revealing a repetitive pattern of coupled pairs of higher-order longitudinal modes. This behaviour is found to be analogue to terrace-like structures formed by interlacing high-frequency symmetric and antisymmetric plate mode curves. A hyperbolic behaviour of curves and modeshape transitions is observed due to mode coupling. The work presented demonstrates analytically how solutions for a thick-walled hollow cylinder correspond to the Lamb wave theory. The relevant pseudo-symmetry relations for mode displacement patterns are obtained using asymptotic approximations of Bessel functions. Theoretical solutions of dispersion characteristics are compared with numerical simulations that are based on the local interaction simulation approach. The results are validated experimentally using laser vibrometry.

1. Introduction

Damage detection methods based on guided ultrasonic waves have been extensively explored for a last few two decades in the field of Non-Destructive Testing (NDT) and Structural Health Monitoring (SHM). This includes methods that utilise Lamb waves propagating in thin plates and Rayleigh waves confined to surfaces of elastic solids [1–3]. Some of these methods are considered for aerospace and civil engineering applications [4–6]. Therefore research effort related to the understanding of guided wave propagation in complex engineering structures is important. In general, any type of geometry in which waves are bounded by one or more surfaces can be regarded as a waveguide. Plates [7] and hollow cylinders [8,9] are examples of waveguides that have attracted considerable attention.

An analytical solution to the problem of elastic waves in an infinitely long, hollow cylinder was firstly introduced in the late 1950s [10]. That initial work included theoretical and numerical analyses of longitudinal, torsional and flexural modes

* Corresponding author at: Department of Mechanical Engineering, The Hong Kong Polytechnic University, Hung Hom, Kowloon, Hong Kong. Tel.: +852 2766 6769.
E-mail addresses: aleksandra.ziaja@connect.polyu.hk (A. Ziaja), li.cheng@polyu.edu.hk (L. Cheng), zhongqing.su@polyu.edu.hk (Z. Su), pawel.packo@agh.edu.pl (P. Packo), lukasz.pieczonka@agh.edu.pl (L. Pieczonka), tuhl@agh.edu.pl (T. Uhl), staszews@agh.edu.pl (W. Staszewski).

http://dx.doi.org/10.1016/j.jsv.2015.04.004
0022-460X/

propagating in the axial direction. Further research work in this area includes studies on ultrasonic waves in hollow cylinders reported in [11,12]. However, research on cylindrical guided waves gained a new impetus when real applications (e.g. related to long distance pipe inspection) were established [8,13,14]. Among various analytical methods developed, the Normal Mode Expansion (NME) technique – introduced in [15] – has made a significant contribution to the analyses of non-axisymmetric cylindrical waves. The NME approach yields the solution to wave propagation problem for a given surface loading. This allows one to determine angular profiles of a pipe at any distance simply as a superposition of excited modes with specific amplitudes [14,16]. From damage detection view point, the physical understanding of various wave modes in monitored structures is of paramount importance as the first step in the development of a new damage detection techniques. It appears that – in contrast to thin-walled hollow cylinders for which research studies have been vibrantly evolving (e.g. research work on crack detection using torsional modes [17], nonlinear wave propagation features [18] or Lamb wave tomography [19]) – very little research work has been conducted for thick-walled cylindrical structures (where the wavelengths suitable for crack detection are much less than the wall thickness). To our knowledge, the work reported in [20] is probably the only literature example, which discusses possible applications of ultrasonic guided waves for crack detection in a thick-walled hollow cylindrical structure: a train axle. However, research developments presented in that work neglect other than Rayleigh waves and thus restrict possible applications only to surface crack detection.

The work presented in the current paper attempts to give a broader theoretical understanding of guided wave propagation phenomena in thick-walled cylindrical structures. Various wave propagation features specific to thick-walled cylindrical structures – such as mode interlacing, pseudo-symmetry of modes and modeshape transitions – are explored and investigated. These phenomena are discussed in relation to the well-established theories. The inner radius of the hollow cylinder is considered as an important parameter that relates obtained solutions to these theories; where in the limits – i.e. for nearly zero and infinite values of the inner radius – the wave propagation theory in plates and solid rods applies, respectively. A paradigm relating wave propagation in hollow cylinders and plates is established analytically using an asymptotic approximation of Bessel functions. Differences, similarities and possible discrepancies in dispersion characteristics and particle displacement patterns are investigated via analytical and numerical studies. The influence of structural geometrical variations on both, i.e. axisymmetric and non-axisymmetric, types of modes is also addressed. Semi-analytical solutions are compared with numerical simulations. The latter is performed using the Local Iteration Simulation Approach (LISA). The results are validated experimentally with the help of laser vibrometry.

The paper is organised as follows. Section 2 starts with the theoretical background, followed by semi-analytical analysis of the paradigm that relates wave propagation in hollow cylinders to wave propagation in plates. Then various characteristic features of axisymmetric and non-axisymmetric modes are discussed using dispersion characteristics. Section 3 presents the results of dispersion characteristics evaluated from numerical simulations. The results are compared with experimental measurements in Section 4. Finally, the work is concluded in Section 5.

2. Guided waves in hollow cylinders – theoretical analysis

Typically, the case of low thickness-to-radius ratio of hollow cylinders is considered in the literature as equivalent to the case of thin-walled pipes. Therefore plate theory approximations are frequently employed when wave propagation is investigated. A more general analysis – that also includes thick-walled structures – is presented in this section. The correspondence between wave propagation in plate and hollow cylinders is demonstrated through semi-analytical analysis. In addition, dispersion characteristics and particle displacements are investigated to reveal mode coupling phenomena.

2.1. Theoretical background

For the clarity of further discussions, a brief introduction to basic notations and expressions used for evaluation of dispersion characteristics is given below. The theoretical derivation presented in this section mainly originates from [10]. For more detailed description readers are referred to [21,22].

For an isotropic hollow cylinder, the wave equation can be derived from the Navier equation given as

$$\mu\nabla^2\mathbf{u}+(\lambda+\mu)\nabla\nabla\cdot\mathbf{u}=\rho\frac{\partial^2\mathbf{u}}{\partial t^2}, \tag{1}$$

where $\mathbf{u}$ is the displacement vector, λ,μ denote Lamé's constants, ρ is the density and ∇^2 is the three-dimensional Laplace operator. When the Helmholtz decomposition is applied, the displacement vector $\mathbf{u}$ can be decomposed into a ϕ-dilatational scalar potential and a $\mathbf{H}$-equivoluminal vector potential, leading to the wave equations

$$v_c^2\nabla^2\phi=\frac{\partial^2\phi}{\partial t^2} \quad \text{and} \quad v_s^2\nabla^2\mathbf{H}=\frac{\partial^2\mathbf{H}}{\partial t^2}, \tag{2}$$

where $v_c=\sqrt{(\lambda+2\mu)/\rho}$ and $v_s=\sqrt{\mu/\rho}$ are the compressional and shear bulk wave velocities, respectively. Assuming waves propagating in positive axial direction of the cylinder (Fig. 1) and denoting the propagation term by $e^{i(\xi z-\omega t)}$ – where ξ and ω are the wavenumber and angular frequency – solutions in the form of radius r and angle θ dependent functions are sought as

$$\phi=f(r)\ \cos\ n\theta\ e^{i(\xi z-\omega t)}$$

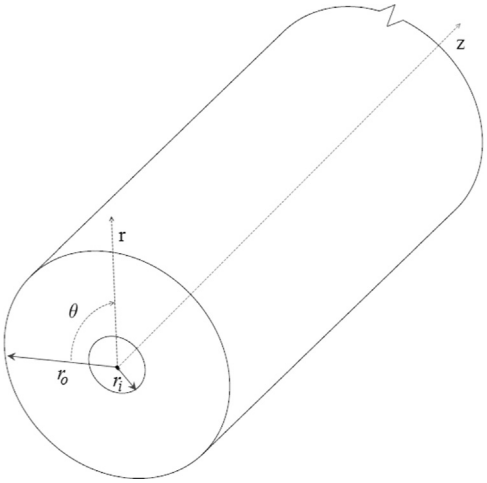

Fig. 1. Cylindrical coordinate system assigned to an infinite cylinder with the inner radius r_i and outer radius r_o.

$$\begin{aligned} H_r &= h_r(r)\ \sin\ n\theta\ \mathrm{e}^{\mathrm{i}(\xi z-\omega t)} \\ H_\theta &= h_\theta(r)\ \cos\ n\theta\ \mathrm{e}^{\mathrm{i}(\xi z-\omega t)} \\ H_z &= h_z(r)\ \sin\ n\theta\ \mathrm{e}^{\mathrm{i}(\xi z-\omega t)}. \end{aligned} \tag{3}$$

Here, one should note that n refers to the circumferential mode order, which for axisymmetric modes is equal to zero and for flexural modes takes integer values from 1 to infinity. In fact this range of possible n values implies that there are double infinite number of modes that can exist in this structure. The general solution to Eq. (1) presented in the form of the radius-dependent functions is recalled in Appendix A.

The traction free boundary conditions, i.e. the stress components σ_{rr}, $\sigma_{r\theta}$ and σ_{rz} at the outer r_o and the inner r_i surface of the cylinder are equal to zero, lead to the characteristic equation of a hollow cylinder in a matrix form

$$|c_{ij}| = 0 \quad \text{for } i,j = 1,2,\ldots,6 \tag{4}$$

where the elements of the first row, corresponding to the stress condition $\sigma_{rr} = 0$ at $r = r_i$, can be found in [10] and in Appendix B.

One can shown that for the axisymmetric modes, i.e. $n=0$, the characteristic equation decouples for the longitudinal $L(0,m)$ and torsional modes $T(0,m)$, where $m = 1,2,\ldots$. The longitudinal modes involve radial u_r, axial u_z displacements, whereas for the torsional modes particles exhibit only angular u_θ translations. For the non-zero circumferential order, i.e. $n = 1,2,\ldots$, the group of flexural modes $F(n,m)$ is obtained.

The dispersion curves can be obtained by semi-analytical evaluation of Eq. (4), for a given inner radius r_i, outer radius r_o and circumferential order n. It is a common practice to draw the dispersion characteristic for combined *thickness-frequency* values. However, dispersion characteristics are presented in this paper for frequency values only to better illustrate the relation between frequency and mode complexity.

2.2. Plate-to-hollow-cylinder relation

It is well known that the plate theory approximations of a hollow cylinder, which are often employed for thin wall pipes, require the radius of the pipe being much larger than the thickness of the wall [14]. This simplification is however invalid for relatively thick-walled tubes, which are investigated in this paper. Thus, in order to establish a connection between the plate and cylindrical guided waves, physical phenomena observed in both types of waveguides are here discussed and compared.

To facilitate the analysis of displacement and stress components, an asymptotic approximation of Bessel functions [23] is applied. Assuming only wave propagation of axisymmetric modes, the general solutions to dilatational f, and equivoluminal h_r potentials from Eq. (3) in the interval of $v_c\xi < \omega$ (for details see Appendices A and C) are reduced to the form given as

$$\begin{aligned} f &= (A+B)\frac{1}{\sqrt{\pi\alpha r}}\ \sin(\alpha r)+(A-B)\frac{1}{\sqrt{\pi\alpha r}}\ \cos(\alpha r) \\ h_r &= (A_1+B_1)\frac{-1}{\sqrt{\pi\beta r}}\ \cos(\beta r)+(A_1-B_1)\frac{1}{\sqrt{\pi\beta r}}\ \sin(\beta r). \end{aligned} \tag{5}$$

Here, α, β are defined as $\alpha^2 = \omega^2/v_c^2 - \xi^2$ and $\beta^2 = \omega^2/v_s^2 - \xi^2$, for the compressional and shear bulk wave velocities denoted respectively as v_c and v_s. By correspondence to the Lamb waves solution, the components with amplitudes $(A-B)$ and (A_1-B_1) can be considered as the pseudo-symmetric parts of the wave, while the $(A+B)$ and (A_1+B_1) as pseudo-antisymmetric parts of the wave. The prefix 'pseudo' refers here to decaying of displacements with the radius.

Grouping all elements into pseudo-symmetrical and pseudo-antisymmetrical parts – the radial and axial displacements take the form

$$u_r = \left[\frac{\alpha}{\sqrt{\pi\alpha r}}\cos(\alpha r)(A+B) - \frac{\xi}{\sqrt{\pi\beta r}}\cos(\beta r)(A_1+B_1)\right] + \left[\frac{-\alpha}{\sqrt{\pi\alpha r}}\sin(\alpha r)(A-B) + \frac{\xi}{\sqrt{\pi\beta r}}\sin(\beta r)(A_1-B_1)\right] \tag{6}$$

$$u_z = \left[\frac{\beta}{\sqrt{\pi\beta r}}\sin(\beta r)(A_1+B_1) + \frac{\xi}{\sqrt{\pi\alpha r}}\sin(\alpha r)(A+B)\right] + \left[\mathrm{i}\frac{-\beta}{\sqrt{\pi\beta r}}\cos(\beta r)(A_1-B_1) + \frac{\xi}{\sqrt{\pi\alpha r}}\cos(\alpha r)(A-B)\right]. \tag{7}$$

The propagation term $e^{i(\xi z-\omega t)}$ was skipped here for brevity. (The general formulae for displacements and stresses are given in Appendix D.)

In order to calculate the displacement vector at surfaces of the cylinder, the relation between the outer r_o and the inner radius r_i in form $r_o = r_i + 2d$ is applied, where d is the half-thickness. Finally, by the transverse resonance principle [21] (partial waves must experience a phase shift of some integral multiple of 2π during the round trip from the outer surface back to the same point) the relations for radial and axial displacements at the outer $u(z, r_o)$ and inner $u(z, r_i)$ surfaces of the cylinder case can be expressed for the pseudo-antisymmetric case as

$$\begin{aligned} u_r(z, r_o) &= \sqrt{\frac{r_i}{r_i+2d}}u_r(z, r_i) \\ u_z(z, r_o) &= -\sqrt{\frac{r_i}{r_i+2d}}u_z(z, r_i) \end{aligned} \tag{8}$$

and for the pseudo-symmetric case as

$$\begin{aligned} u_r(z, r_o) &= -\sqrt{\frac{r_i}{r_i+2d}}u_r(z, r_i) \\ u_z(z, r_o) &= \sqrt{\frac{r_i}{r_i+2d}}u_z(z, r_i). \end{aligned} \tag{9}$$

The results show that for the inner radius approaching infinity or the thickness being sufficiently small comparing to r_i, the Lamb wave mode symmetry and antisymmetry relations can be obtained. (Exemplary results illustrating displacements patterns will be given in Section 2.4.)

In contrast to the plate solution (i.e. Lamb waves), the stress components in a hollow cylinder do not follow the symmetry or pseudo-symmetry. This can be also presented with the asymptotic approximation approach as it was done in the case of the displacements. The approximated radial and axial stress components are given as

$$\sigma_{rr_{\mathrm{p-sym}}}(r) = \frac{\mu}{\sqrt{r}}\left\{\frac{1}{\sqrt{\pi\alpha}}\left[-\left(\beta^2-\xi^2\right)\cos\alpha r + \frac{2}{r}\alpha\sin\alpha r\right](A-B) + \frac{1}{\sqrt{\pi\beta}}\left[2\xi\beta\cos\beta r - \frac{2}{r}\xi\sin\beta r\right](A_1-B_1)\right\} \tag{10}$$

$$\sigma_{rz_{\mathrm{p-sym}}}(r) = \mathrm{i}\frac{\mu}{\sqrt{r}}\left\{\left[-2\xi\alpha\frac{1}{\sqrt{\pi\alpha}}\sin\alpha r\right](A-B) + \left[\left(\xi^2-\beta^2\right)\frac{1}{\sqrt{\pi\beta}}\sin\beta r\right](A_1-B_1)\right\}. \tag{11}$$

(It is important to note that here, only the components of $(A-B)$ and (A_1-B_1) terms, i.e. pseudo-symmetrical displacements, are studied; the relevant stresses for pseudo-antisymmetrical components follow the same procedure.) Comparison of stresses at the inner and outer surfaces of the cylinder shows the pseudo-symmetry for axial stresses, i.e.

$$\sigma_{rz_{\mathrm{p-sym}}}(r_o) = -\sqrt{\frac{r_i}{r_i+2d}}\sigma_{rz_{\mathrm{p-sym}}}(r_i). \tag{12}$$

However, one can notice that the corresponding relation is not valid for the radial component of stress, due to the $(2/r)\alpha\sin\alpha r$ and $(2/r)\xi\sin\beta r$ terms in Eq. (10). These coupling terms are inversely proportional to the cylinder radius. At the limiting case of $r\to\infty$, the problem converges to the well-known Rayleigh–Lamb relations.

It is important to note that although the accuracy of the evaluated displacement and stress formulae is increasing with mode order, some limitations apply here. These limitations concern the Bessel function approximations, such as for the case of the radius equal to zero (i.e. for a solid cylinder case). Also, since only the first and second kind Bessel functions were

considered here, the discussion corresponds to phase velocities above the compressional bulk velocity. However, the intention was to investigate the characteristic features of hollow cylinder modes in correspondence to the well-developed Lamb waves theory, thus the approach that relates the Bessel functions of cylindrical structures with cosine/sine functions of a plate was chosen.

2.3. Influence of geometrical parameters on dispersion characteristics

In the work on non-axisymmetric guided waves in large-diameter pipes, reported in [14], the argument is given that waves in a hollow cylinder can be treated as Lamb waves propagating in an unwrapped plate, under the assumption that the diameter of the cylinder is much greater than its thickness. The authors point out that the similarity between behaviour of Lamb waves and cylindrical guided waves is also frequency dependent. Thus, the division of dispersion plots into the lower frequency region (where the wall thickness is much lower than the wavelength) and the higher frequency region (where the wavelength is comparable to or less than the wall thickness) was proposed. However, this frequency-related separation was based only on visual comparison of phase velocity of corresponding plate and cylinder modes, and neither an explicit condition nor an error estimate has been proposed.

In this section differences between the dispersion characteristics for a thin- and a thick-walled hollow cylinder are presented. For the sake of clarity, firstly the relation between a thin-walled and a thick-walled structure needs to be established.

In common engineering practice (e.g. for pressurised cylinders), the thin wall assumption requires that the radial stress component in the wall is negligibly small when compared with the tangential and axial components; this is typical for structures of thickness not larger than 1/10 of the diameter [24]. In the ultrasonic wave propagation analysis the strict division upon thin and thick wall structures has not been clearly stated in the literature; however, the influence of the Mean Radius-to-Thickness (MRT) and the Thickness-to-Wavelength Ratio (TWR) on dispersion characteristics can be summarised with the two following observations [25,26]: (i) the TWR is a determining factor for the nature of dispersion curves; (ii) as the MRT ratio tends to infinity the solution uncouples for Rayleigh–Lamb and shear horizontal waves of infinite plate waves. Fig. 2 illustrates the MRT variation on a longitudinal mode dispersion spectrum. In this example, the wall thickness of the cylinder is kept constant (75 mm) and the MRT ratios of 0.6, 1, and 5 were selected for the analysis. In addition, the dispersion curves for a plate of the same thickness and solid cylinder with radius 75 mm are presented in the same figure. One should note that the Lamb waves solution can be considered as the limiting case for a hollow cylinder with the infinite mean radius.

The results show that the higher-order curves of different MRT parameters (except the solid cylinder modes) become indistinguishable and follow a similar pattern. On the other hand, the sensitivity of the curves to the MRT parameter is relatively large in the low frequency range, where wavelengths are of the same order as the wall thickness of the cylinder. Since the thickness was held constant throughout the entire analysis the key factor influencing the phase velocity is the curvature.

The analysis of the results in Fig. 2 also points out that the parameter determining the nature of dispersion characteristics is the MRT-to-frequency ratio, which represents the relationship between the wall thickness, cylinder radius and excitation frequency. This observation implies that when damage detection applications were considered in thick-walled cylindrical structures (for which wavelengths suitable for crack detection are much less than the wall thickness) the curvature influence on dispersion of axisymmetric modes would be relatively small. For such cases the classical plate theory seems to provide a very useful approximation of dispersion characteristics. Despite only small differences in phase velocities between a hollow cylinder and a plate, the relevant particle displacement distributions along the radial direction are significantly different (to be illustrated in the following section). Therefore, the approximations suitable for the analysis of thin-walled large diameter pipes cannot be simply used for high frequency waves in an arbitrary cylinder. This implication is important when damage detection in such cylinders is considered.

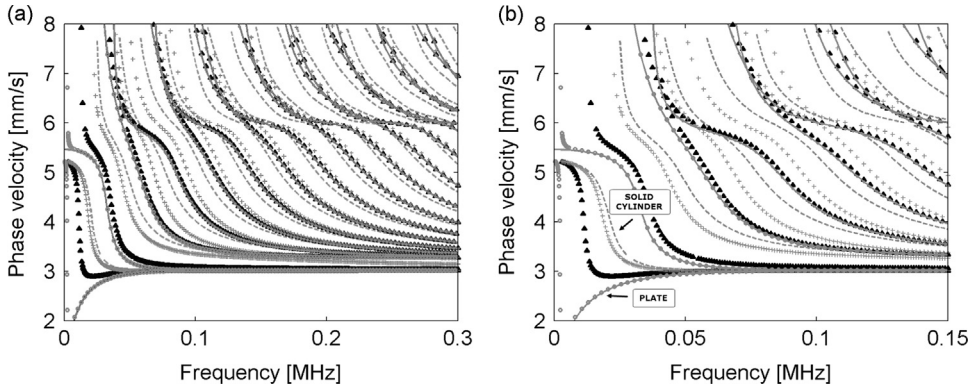

Fig. 2. Mean Radius-to-Thickness (MRT) parameter influence on phase velocity dispersion curves for a steel hollow cylinder of wall thickness equal 75 mm in: (a) broad spectrum range, (b) zoomed view displaying lower-order modes. Only the longitudinal modes are shown for the MRT equal to: ∞ (solid line —; these are the Lamb wave modes); 5 (○ symbols); 1 (△ symbols); 0.6 (+ symbols); 0.5 (dashed line – –; these are the solid cylinder wave modes).

2.4. Modes interlacing phenomenon

The study related to the influence of the MRT parameter on phase velocity dispersion curves has revealed a regular pattern in the behaviour of higher-order axisymmetric modes for a hollow cylinder. This section investigates the characteristic features related to this behaviour. The discussion of dispersion plots follows the order from high to low phase velocity values (i.e. the increasing wavenumber order).

An example of numerically evaluated dispersion characteristics of axisymmetric modes is illustrated in Fig. 3.

The results show that except the first few wave propagation modes, pairs of longitudinal modes seem to interlace in the phase velocity range above the compressional bulk wave velocity (v_c=5960 m/s for steel) and separate below this phase velocity limit. This behaviour is identical for all higher-order modes regardless the geometrical parameters of the cylinder, as discussed in the previous section. The exemplary higher-order pseudo-symmetric and antisymmetric longitudinal mode shapes – evaluated from the exact solution of the characteristic equation – are presented in Fig. 4. For the case investigated – i.e. for the inner radius equal to 25 mm and the wall thickness equal to 75 mm – the amplitudes of radial and axial displacements at the inner surface of the cylinder are about twice the value of the displacements at the outer surface, as expected from Eqs. (8)–(9).

When the relations for thick plates and thick wall cylinders – discussed in Sections 2.3 and 2.2 – are recalled, the dispersion curve interlacing phenomenon can be examined here more closely, following the elaboration on higher-order plate modes and the so-called terrace-like structures [27].

It is known that pairs of interlacing higher-order symmetric and antisymmetric Lamb modes, bounded by mixed-boundary modes, form the terrace-like structures in dispersion characteristic. The Lamb modes intersection points satisfy both traction-free and mixed-boundary condition [27]. Although the pseudo-symmetric and pseudo-asymmetric longitudinal modes of a hollow cylinder can be differentiated according to the displacement patterns, the pairs of modes are coupled via radial stress components, as discussed in the previous section. This coupling manifests itself in the dispersion characteristics by a hyperbolic (non-crossing) behaviour of the curves in the coupling region, as shown in Fig. 5(a).

These observations are consistent with the classical understanding of coupled system spectrum behaviour [28]. In the coupling regions, the displacement patterns assigned to a single dispersion curve exhibit transitions between pseudo-symmetric and pseudo-antisymmetric character as depicted in Fig. 6.

The interlacing of longitudinal modes can be also studied from the point of view of the group velocity. This velocity corresponds to the rate of energy transfer in a structure. Fig. 5(b) illustrates the interchanging of group velocities for two longitudinal modes in the analysed coupling region. It appears that for hollow cylinder longitudinal modes, there is no energy transfer between the two coupled modes and the energy associated with each of the modes travels with the same rate v_g. (In contrast, for an uncoupled set of modes, e.g. Lamb waves, the crossings of dispersion curves in a phase velocity spectrum correspond to the local minima and maxima of the modes group velocities, i.e. resonances and anti-resonances of the modes, and imply back and forth energy transfer between modes [29].)

For frequencies below the modes interlacing region in the phase velocity dispersion curves, another interesting feature can be observed. For higher-order pseudo-symmetric modes, the plateau regions around compressional wave velocity can be noticed (Fig. 3). This local phase velocity flat character implies that the group velocity at this region is nearly constant, with an actual value slightly below the compressional bulk wave velocity. Any excitation of modes at this narrow frequency range will result in propagation of almost a non-dispersive wave with a dominant compressional wave component. The described behaviour can be understood as equivalent to the plateau regions observed in the past for solid cylinders [30] and high-order Lamb modes [27,29].

When higher frequencies are analysed, all longitudinal modes – except the $L(0,1)$ and $L(0,2)$ modes – tend to the shear bulk wave velocity, whereas the phase velocity of the two lowest longitudinal modes approaches the Rayleigh waves velocity and form displacement behaviour comparable to surface waves, i.e. waves concentrated at the vicinity of the inner/outer surfaces of the cylinder.

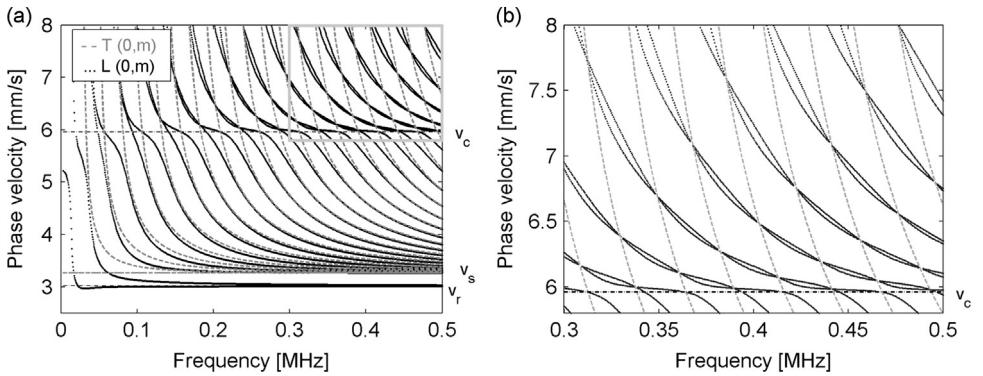

Fig. 3. Numerically evaluated dispersion characteristics for axisymmetric modes in a steel hollowed cylinder (inner radius – 25 mm; thickness – 75 mm): (a) repetitive pattern of longitudinal $L(0,m)$ and torsional $T(0,m)$ wave modes; (b) terrace-like structures of 'interlacing' $L(0,m)$ modes. The dashed-dot ($-\cdot$) lines indicate the Rayleigh (v_r), shear (v_s) and compressional (v_c) bulk wave velocity limits.

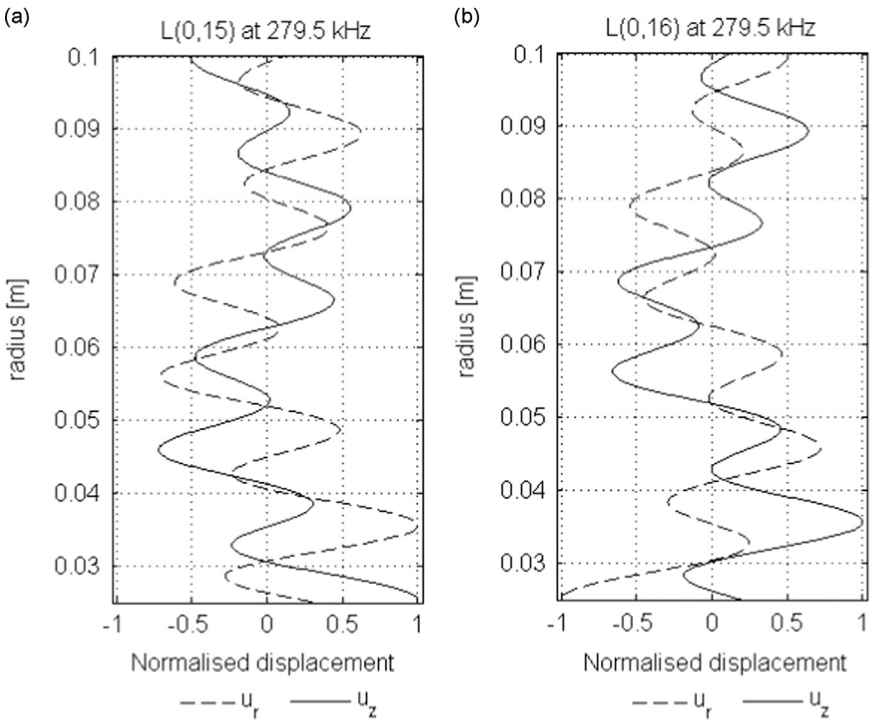

Fig. 4. Comparison of normalised displacement plots in the axial u_z and radial u_z direction for a steel hollow cylinder (inner radius equal to 25 mm; thickness equal to 75 mm): (a) pseudo-antisymmetric $L(0,15)$ mode; (b) pseudo-symmetric $L(0,16)$ mode.

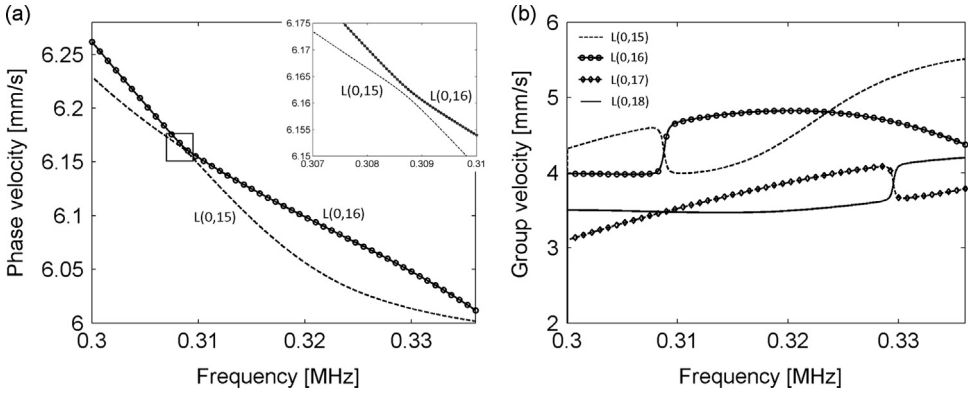

Fig. 5. (a) Hyperbolic behaviour of a pair of longitudinal modes in a mode coupling region (one should refer to Fig. 3 for the wider phase velocity spectrum); (b) group velocity interchanging behaviour.

2.5. Flexural modes

So far, only the axisymmetric modes, i.e. longitudinal $L(0,m)$ and torsional $T(0,m)$, were considered. However, as shown in [16], any partial loading results in the excitation of both, i.e. longitudinal and flexural, $F(n,m)$ modes. Thus, a brief study on non-axisymmetric modes in thick wall cylinders is presented in this section. Fig. 7 illustrates a change in the nature of the dispersion curves with an increase of the circumferential order. Due to the complexity of the results, the dispersion curves presented were calculated numerically with the fine resolution of 0.1 rad/m in the wavenumber domain and the frequency step of 500 Hz.

The flexural modes dispersion characteristics for thick-walled cylinders are significantly different from thin-walled cylinders (compare Fig. 7 with Fig. 8). The phase velocity–frequency curves for thin-walled cylinders seem to follow the pattern of the axisymmetric modes, deflecting to higher phase velocity values with the increase of the circumferential order in the lower frequency range and converging to a single pattern for higher frequencies. On the other hand, for a thick-walled cylinder, the higher circumferential order results in unravelling of the lower flexural modes as marked by a dashed circle in Fig. 7.

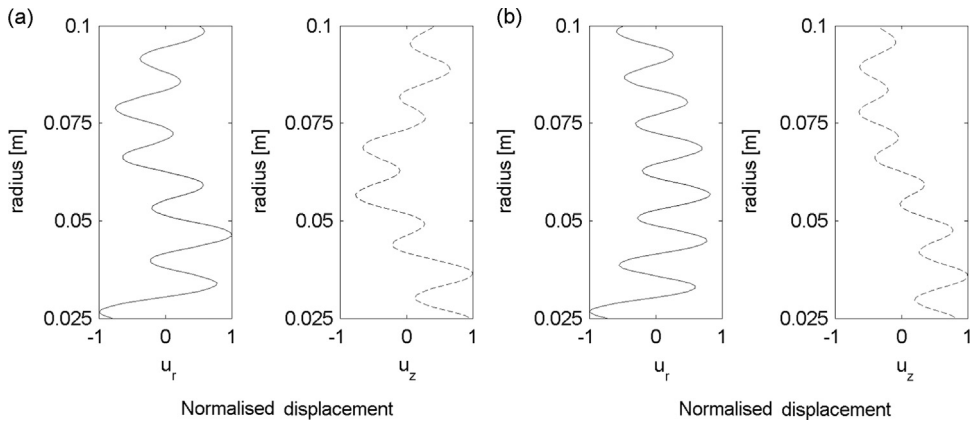

Fig. 6. Change of the mode character alongside the $L(0,16)$ dispersion curve. Displacement patterns for the frequency: (a) 290 kHz, (b) 320 kHz. The results were calculated using the DISPERSE® software.

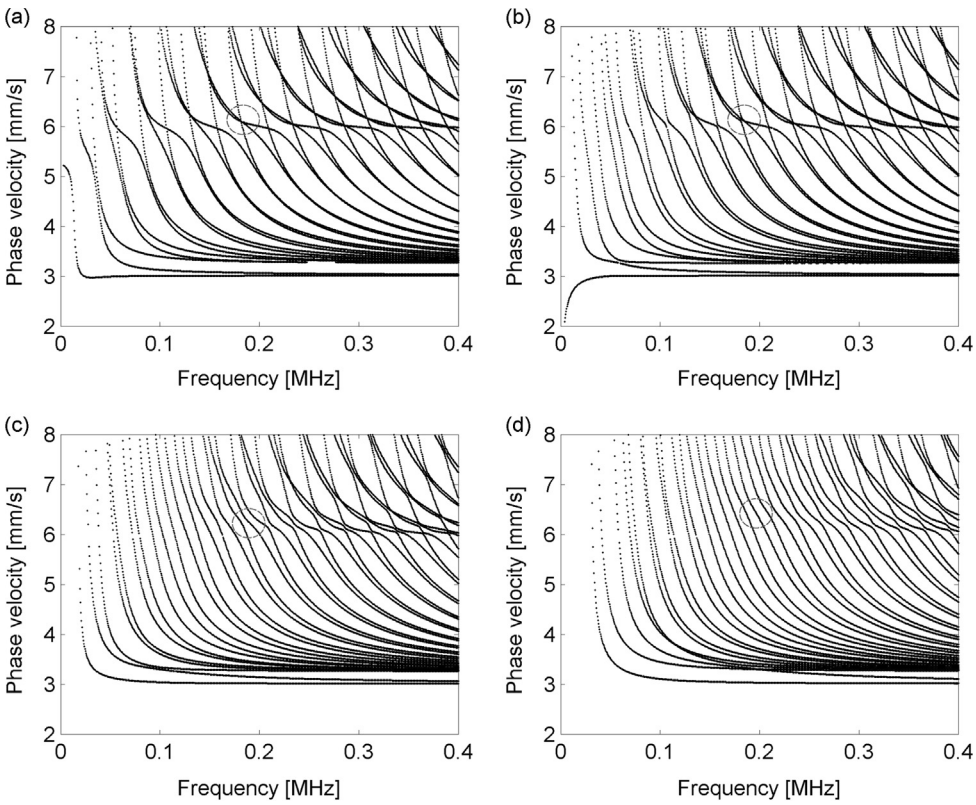

Fig. 7. Comparison of dispersion curves for axisymmetric $n=0$ and non-axisymmetric $n=1,3,5$ modes for a steel hollow thick-walled cylinder (inner radius equal to 25 mm; thickness equal to 75): (a) longitudinal and torsional modes; (b) $F(1,m)$ mode; (c) $F(3,m)$ mode; (d) $F(5,m)$ mode. (a) circumferential order $=0$, (b) circumferential order $=1$, (c) circumferential order $=3$ and (d) circumferential order $=5$.

It is also important to note that in contrast to torsional and longitudinal modes, the flexural modes do not intersect with each other but instead follow a hyperbolic behaviour as illustrated in Figs. 8 and 9. The results also indicate the coupling between the three consecutive flexural modes analysed. The coupling depends on the geometrical parameters and decreases with an increase of the MRT parameter. In addition, a transition of the dominant mode character along the curve – analogues to the one discussed previously for the coupled longitudinal modes – can be observed.

2.6. Summary

The elastic wave propagation behaviour in a hollow cylinder has been investigated theoretically using the analysis of dispersion characteristics and particle displacement patterns. The most important observations and their implications for damage detection applications can be summarised as follows.

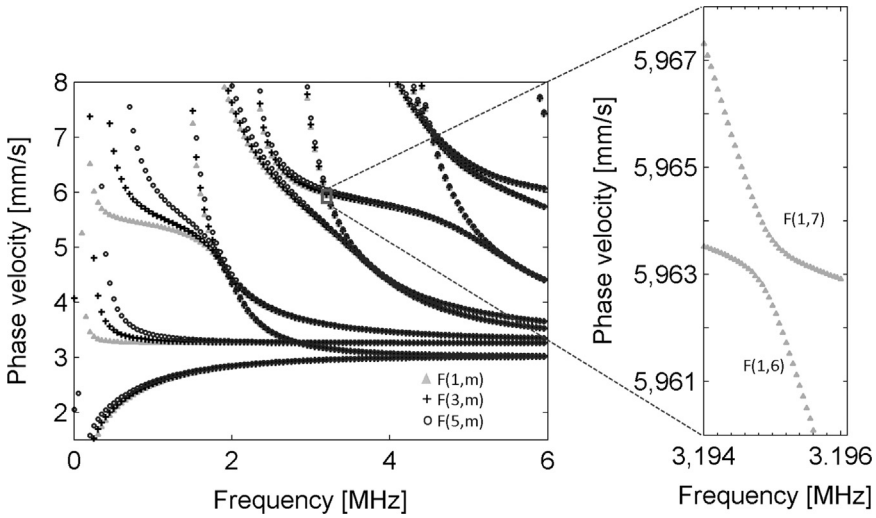

Fig. 8. Comparison of higher circumferential order $F(1,m)$, $F(3,m)$ and $F(5,m)$ modes in a steel hollow thin-walled cylinder (inner radius equal to 8.2 mm, thickness equal to 1.22 mm).

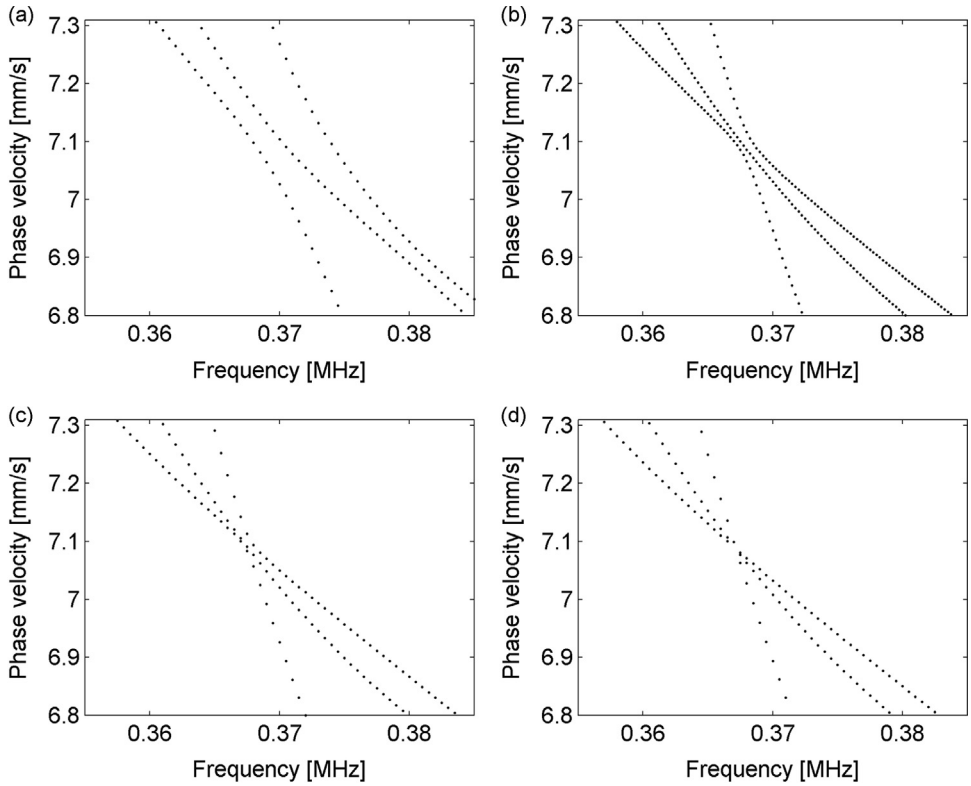

Fig. 9. Hyperbolic behaviour of flexural modes $n=1$ in a mode coupling region (cylinder wall thickness equal to 75 mm): (a) MRT=0.6, (b) MRT=0.8, (c) MRT=1, (d) MRT=5.

In theory, a double infinite number of dispersive modes can propagate in an axial direction of any hollow cylinder structure. The analysis shows that the complexity of wave modes increases significantly for thick-walled cylinders. This complexity becomes a real challenge when damage detection methods – based on elastic wave propagation – need to be developed and implemented in such structures. Although numerous multiple wave modes can propagate in thick-walled cylinders, a common pattern – analogues to the terrace-like structures in plates – has been observed in the dispersion characteristics for higher-order axisymmetric modes above the frequency range corresponding to the compressional bulk velocity limit. For this high frequency region, relevant wavelengths are significantly smaller than the cylinder wall thickness.

Therefore the cylinder's curvature will manifest its effects only by the coupling between the modes. In the low frequency region, the mean radius-to-thickness ratio has been identified as an important geometrical parameter, which influences the shape of the dispersion curves.

The analysis of displacement patterns points out the pseudo-symmetry of the longitudinal modes across the wall thickness. It is important to note that although the findings of the research presented in this section are similar to the conclusions reached in [18] for thin-walled pipes with a high radius approximation, a more general case of hollow cylinder – with an arbitrary radius and wall thickness – was considered here. In practice, the pseudo-symmetry implies that in general, larger displacements for a given mode are expected at the inner rather than the outer surface of the cylinder.

3. Numerical simulations

Following the theoretical analysis and discussion on dispersion characteristics of hollow cylindrical guided waves, numerical simulations were performed to evaluate wave propagation responses to broadband excitation. To obtain dispersion characteristics – broadband excitation scenario – various numerical approaches can be used (e.g. finite element method [31] or semi-analytical finite element (SAFE) method [32]). In this work, numerical simulations were carried out using the Local Interaction Simulation Approach (LISA) [33–36]. The use of a model-based LISA allowed to simulate the excitation-sensing procedures as expected in the experimental investigations. Parallel processing architecture of the LISA algorithm was used and graphical card technology (CUDA) employed to reduce the computational effort [37]. The geometry in numerical simulations corresponded to the setup used in the analytical model. The cylinder was 250 mm long, with an inner radius of 25 mm and a wall thickness of 75 mm. The cylinder was meshed using 0.5 mm cubic elements. This resulted in the total number of 65M elements and 195M degrees of freedom. Material properties equivalent to aluminium were assumed, i.e. Young's modulus $E=70$ GPa, Poisson ratio $\nu=0.3$ and density $\rho=2700$ kg/m^3. Time step was equal to 0.05 μs to ensure the stability of the explicit time integration algorithm.

The excitation was introduced as out-of-plane displacement for a single node. Displacement responses were acquired at selected nodal points during the simulation. Several calculations were performed in order to determine the most convenient measurement conditions, and to investigate various guided waves propagation properties.

3.1. Results for broad-band excitation – dispersion characteristics

Firstly, wideband excitation was used to estimate dispersion characteristics. A chirp signal covering the frequency range from 50 to 150 kHz was used in order to maximise the energy of the input signal. Two excitation points – located close to the inner and outer edges of the cylinder – were selected. In both cases, the responses were acquired at the outer surface along a line parallel to the cylinder's axis. Altogether 471 responses were gathered in the simulations. The response time was set to 0.5 ms, allowing for double wave reflections from the flat end surfaces. Simulated signals were processed using a two-dimensional Fourier transform resulting in the wavenumber–frequency representation, i.e. the dispersion characteristics. The results for the two considered excitation scenarios are presented in Fig. 10(a) and (b). The brighter colours indicates the higher amplitudes.

The results show that for the two excitation scenarios used (i.e. inside and outside wave excitation) a complex pattern of multi-modal wave propagation can be observed. Both analyses display the strong Rayleigh wave at the outer surface, as indicated by a straight diagonal line. These results can be compared with the analytical solution given in Fig. 10(c). A significant difference in the distribution of wave amplitudes can be also observed when the results for the two simulated excitation scenarios are compared. Once a large portion of the energy – introduced by the transmitter at the outer surface – is carried by the Rayleigh wave mode, its amplitude dominates the wavefield. Fig. 10(b) for the outside excitation demonstrates that, except for the Rayleigh mode and higher amplitudes in the low frequency range, no clear mode can be distinguished. On the other hand, when the inside excitation is used, the wavefield recorded at the outer cylinder surface shows a number of higher-order modes of similar amplitudes to the amplitude of the Rayleigh wave. This behaviour is manifested in Fig. 10(a) as a pattern of parallel curves above the compressional velocity line.

3.2. Summary

Numerical simulations reveal a number of wave propagation modes in the dispersion characteristics of the thick-walled hollow cylinder. However, these characteristics are dominated by the Rayleigh mode. The results show that the excitation inside the cylinder produces better results than the excitation outside the cylinder as it facilitates propagation of the higher-order modes, allowing for inspection of the cylinder's wall throughout its thickness.

Since both antisymmetric and flexural type of modes are present in the dispersion characteristics, a very fine resolution in the wavenumber domain would be required in practical applications to differentiate between various wave propagation modes. However, in practice this fine resolution is limited by the length of the array of transducers placed at the outer surface and in consequence by the total length of the cylinder. Therefore, in order to obtain more accurate dispersion curves the analysis of longer cylinders will be required in practice. The number of the propagating modes can be also restricted (e.g. to longitudinal modes only) by excitation with an array of transducers.

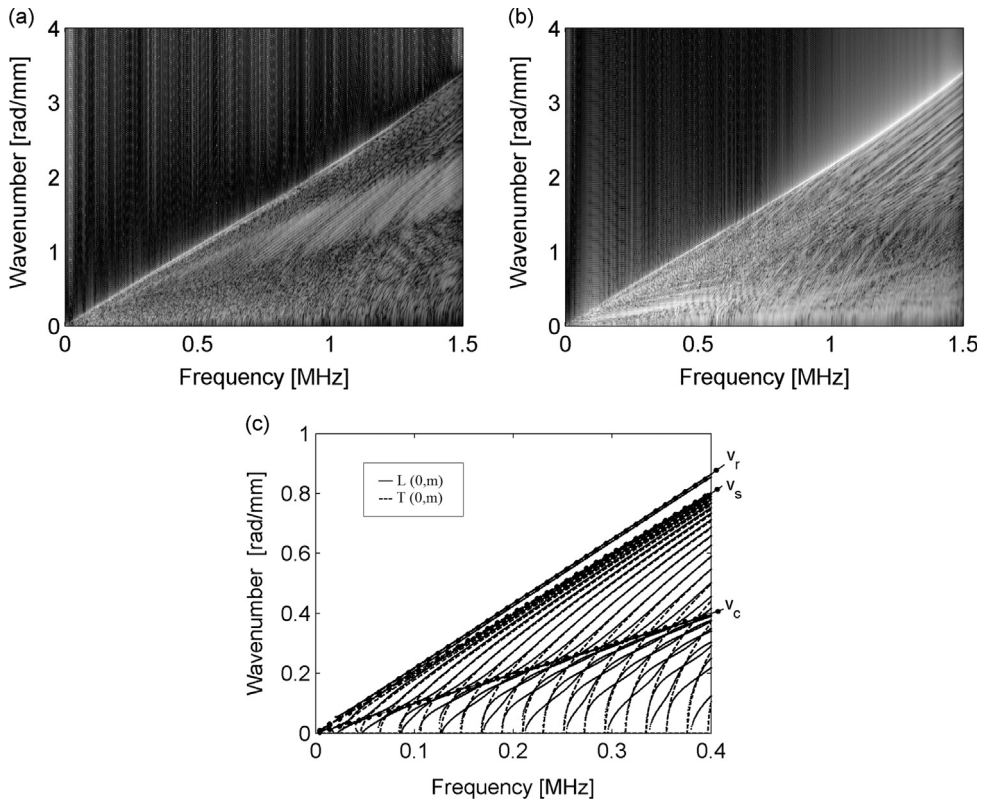

Fig. 10. Dispersion characteristics of a steel hollowed cylinder (inner radius – 25 mm; thickness – 75 mm): (a) simulation-based with inner surface excitation; (b) simulation-based with outer surface excitation; (c) theoretical axisymmetric modes (Eq. (4)). The dot-dashed ($-\cdot$) lines indicate the Rayleigh (v_r), shear (v_s) and compressional (v_c) bulk wave velocity limits.

4. Experimental validation

This section presents results from a series of experiments conducted to validate numerical simulation results. Experimental arrangements used are described firstly. Then experimental results are presented to reveal opportunities and limitations related to wave propagation scenarios that could be used for structural damage detection.

4.1. Experimental arrangements

A hollowed aluminium cylinder of total length of 500 mm, inner radius of 25 mm and wall thickness of 75 mm was used in the experiments (Fig. 11). The inner radius and wall thickness were the same as in numerical simulations. Two piezo-stack NOLIAC transducers of $2 \times 2 \times 2$ mm were used for wave excitation. The transducers were bonded to the inner and outer surfaces of the cylinder using a two-component adhesive glue. The location of the transducers is shown in Fig. 11(b).

Wave propagation responses were captured using two non-contact measuring systems, i.e. one-dimensional (1-D) *Polytec PSV-400* and three-dimensional (3-D) *Polytec PSV-400-3D* scanning laser vibrometers. Both laser vibrometers were controlled using a PC. The *RoboVib Structural Test Station* – that uses an industrial *KUKA* robot – was employed to automate positioning of the heads of the 3-D scanning laser vibrometer. Fig. 12 shows the experimental set-ups used for the dispersion characteristic estimates and wave propagation analysis. The experimental work involved the same wave propagation scenarios, parameters and data processing as used in numerical simulations.

The first experiment involved two excitation scenarios, i.e. the excitations with the transducer located on the outer and inner surfaces of the cylinder. A chirp signal was used for excitation. The sweeping frequency of the chirp runs from 50 to 800 kHz. The total duration of the chirp excitation signal was 250 μs. The out-of-plane wave propagation response signals were measured using the 1-D scanning laser vibrometer. The response measurements were taken at 400 points located on the outer-surface of the cylinder, alongside the line parallel to its axis of symmetry. These velocity measurements were taken with the spatial resolution of 1 mm and acquired using the sampling frequency of 5.12 MHz. All signal responses were averaged using 100 data records in order to improve the signal-to-noise ratio.

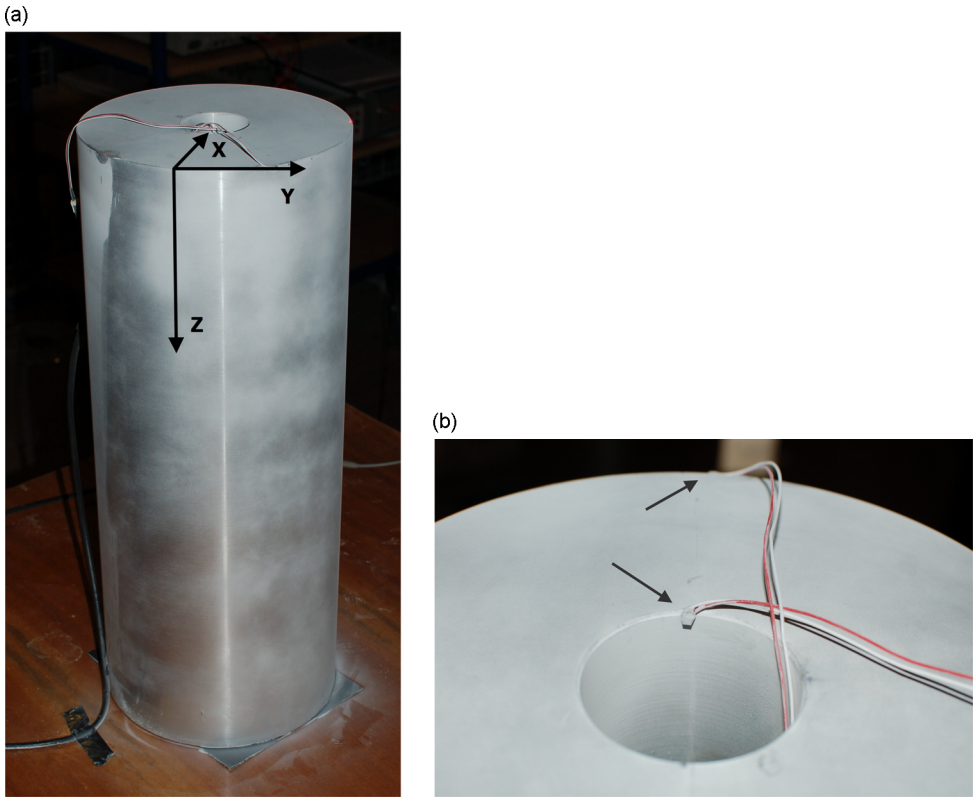

Fig. 11. Thick hollowed aluminium cylinder used in experimental investigations: (a) general view with a 3-D coordinate system used in measurements; (b) locations of transducers used for wave excitation.

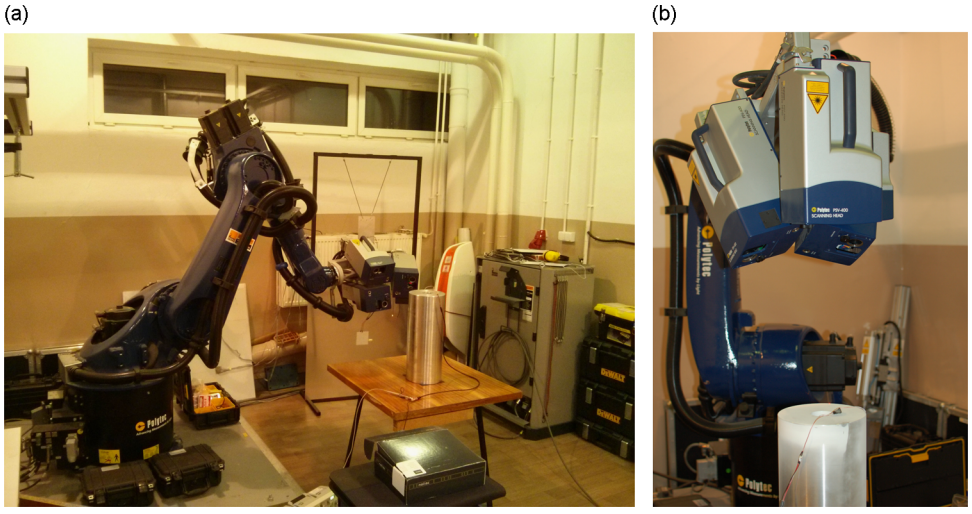

Fig. 12. Experimental set-ups used for (a) dispersion characteristic estimates; (b) wave propagation analysis.

4.2. Experimental results

4.2.1. One-dimensional measurements

The dispersion characteristics were obtained by applying the two-dimensional Fourier Transform to the response data. The Hanning window was used to reduce the leakage effect in the involved Fourier spectra. Fig. 13(a) presents the results for the outer surface excitation scenario. The black dashed lines in this figure correspond to the theoretical velocity limits for guided (Rayleigh) and bulk (shear and compressional) wave propagation in aluminium. The experimental dispersion characteristics shown in Fig. 13 can be compared with the relevant analytical characteristics given figure in Fig. 10(c).

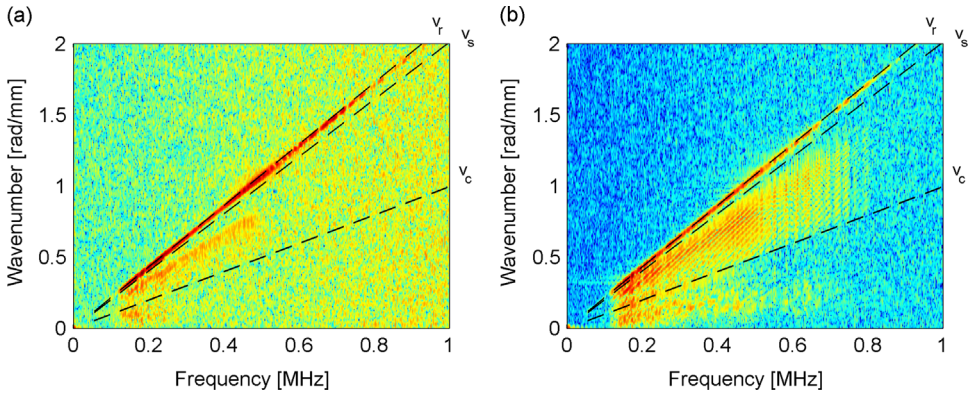

Fig. 13. Experimental wavenumber–frequency dispersion characteristics evaluated from the 1-D response data resulting from: (a) the outer surface excitation; (b) the inner surface excitation. The dashed (– –) lines indicate the velocity limits for the guided Rayleigh wave (v_r), shear bulk wave (v_s) and compressional bulk wave (v_c).

In order to minimise the influence of circumferential surface waves on other wave modes, the windowed time signals of 0.3 ms were also used to evaluate the dispersion characteristics. The results for the outer surface excitation exhibit strong (high amplitude) Rayleigh wave modes. The displacements of these modes are confined to the cylinder surfaces. Additional modes with higher amplitudes can be observed in the region between the shear wave and the compressional wave limits. However, it is very difficult to distinguish (or separate) between these consecutive modes. Interestingly, when the inner surface excitation was used the dispersion characteristics are significantly different, as demonstrated in Fig. 13(b). On top of the strong surface wave modes, a number of higher-order modes – closely spaced in the wavenumber domain – can be observed in the 200–700 kHz frequency range. There are two explanations behind the differences in the dispersion characteristics obtained using the outer and inner excitations. The experimental tests have demonstrated that for the outer excitation the strong outer-surface waves mask the higher-order cylinder modes, and the inner excitation better excites the flexural modes. It is also important to note that due to relatively weak piezo-based excitation – that was used intentionally – the results above 500 kHz are noisy and the mode behaviour is blurred.

4.2.2. *Three-dimensional measurements*

Additional experimental tests were performed to verify dispersion characteristics and to identify the dominant wave components. The 3-D scanning laser vibrometer was used in these tests in order to obtain the velocity responses in the *X* (normal), *Z* (axial) and *Y* (tangential) directions. The results are presented in Appendix E.

The results are in good agreement with the 1-D measurements discussed in the previous section. The out-of-plane measurements exhibit the strongest amplitudes in the dispersion characteristics for both outer and inner surface excitations. Again, the surface wave components are dominant in these out-of-plane characteristics. In addition, weak amplitudes of the axial and tangential wave components can be also observed in the dispersion characteristics, particularly for the inner surface excitation. This confirms the previous finding that the inner surface excitation leads to stronger flexural modes. It is important to note that the torsional modes were not excited by the piezo-transducers used in the experimental tests.

The existence of waves propagating in the circumferential direction (with high amplitudes confined to the outer surface of the cylinder) was confirmed by the experimental tests, as illustrated in Fig. 14(b). The outer surface excitation – involving the 200 kHz ten-cycle sine wave enveloped by the Hanning window – was used in these tests. The secondary wave packets – induced by the circumferential waves and propagating in the axial direction – were also observed as shown in Fig. 15. When the inner-surface excitation was used, the strong (i.e. high-amplitude) wavefront – travelling across the wall of the cylinder – can be observed in Fig. 14(a).

4.3. *Summary*

The experimental results presented in this section confirm the numerical simulation results. It is clear again that the Rayleigh wave modes – with high amplitudes confined to the surfaces – are the dominant wave propagation modes in the thick hollow cylinder. Also, there are significant differences in the evaluated dispersion characteristics when the two excitation scenarios (i.e. outer-surface and inner-surface excitations) are used. The experimental results reveal a complex pattern of high-order modes for the single-point, inner-surface excitation. Although, these multiple and interlacing modes are difficult to separate, some information can be obtained with respect to the range of velocities involved in the propagation of these modes.

Interestingly, a strong pattern of interlacing modes in the high-resolution dispersion characteristics – obtained for a thin plate – was observed previously in [38].

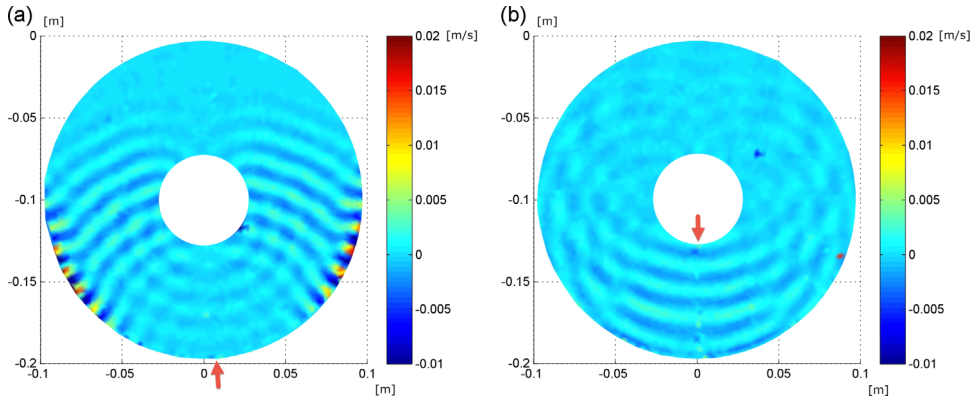

Fig. 14. Experimental wave propagation out-of-plane velocity patterns acquired after 0.1 ms for: (a) outer-surface excitation; (b) inner-surface excitation. The excitation points are marked with the arrows.

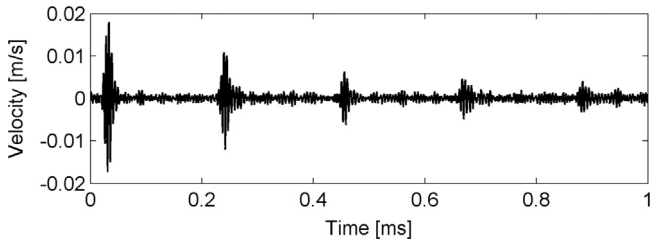

Fig. 15. Experimental out-of-plane response velocity signal displaying the secondary wave packets induced by the circumferential waves. The outer-surface signal was acquired 1 mm below the outer-surface excitation point.

5. Conclusions

Elastic waves guided by thick-walled, hollow cylindrical structures have been investigated. Theoretical, numerical and experimental investigations have been undertaken to facilitate understanding of various wave propagation phenomena in thick-walled cylinders. Firstly, the semi-analytical analysis was performed to investigate the characteristic features of guided modes and to establish the correlation between thick plate and cylinder waveguides. Then numerical simulations and experimental tests were used to investigate outer- and inner-surface excitation scenarios for potential damage detection applications. The major conclusions from all these investigations can be summarised as follows.

Theoretical investigations reveal a complex pattern of wave modes in thick-walled cylinders. Despite this complexity of modes, a common pattern of higher-order axisymmetric modes – analogous to terrace-like structures in plates – has been observed in the dispersion characteristics, above the compressional wave velocity limit. Since the relevant wavelengths are significantly smaller in this high-frequency region, the cylinder's curvature will manifests its effects only through the coupling between the modes. The theoretical analysis of displacement patterns demonstrates the pseudo-symmetry of the axisymmetric longitudinal modes across the wall thickness. The theoretical study also reveals that the weak coupling between pairs of consecutive longitudinal modes – caused by the radial stress component – results in a hyperbolic behaviour of the dispersion curves in the mode interlacing region, i.e. above the compressional wave velocity limit.

Numerical simulations and experimental tests also reveal a complex pattern of seemingly interlacing wave propagation modes in the dispersion characteristics of the thick-walled hollow cylinder. There are significant differences in the evaluated dispersion characteristics when the two investigated excitation scenarios – i.e. the outer-surface and inner-surface excitations – are used. The analyses also show that the Rayleigh wave modes – with high amplitudes confined to the surfaces – are the dominant wave modes in the thick hollow cylinder. However, the amplitude of the surface Rayleigh wave is weaker when the inner-surface excitation is used.

The results of the investigations demonstrate that damage detection based on ultrasonic wave propagation is possible in thick-walled hollow cylinders. However, any practical application will require thorough understanding of complex wave propagation phenomena involved and appropriate monitoring strategies (i.e. excitation sources, positions and frequencies). It is well known that good damage detection sensitivity will require high-frequency excitation to obtain wave propagation modes with shorter wavelengths. The study reveals that the Rayleigh waves are dominant in the high-frequency region, restricting possible inspections to surface and sub-surface damages. However, for inner surface excitations, amplitudes of the Rayleigh waves are much weaker on the outer surface of the cylinder than for the outer-surface wave excitation. Since additionally the excitation inside the cylinder produced better results in terms of excitation of the higher-order modes than the excitation outside the cylinder, the inner-surface excitation appears to be superior for damage detection applications.

Finally, it is clear that further – particularly experimental – studies are required by involving different types of transducers, excitation positions and frequency ranges. The preliminary findings of this paper are expected to facilitate future investigations towards the establishment of the effective damage detection method for thick-walled hollow cylinders.

Acknowledgements

The work presented in this paper was supported by the National Natural Science Foundation of China (Grant no. 11272272). The last author would like to acknowledge the financial support from the Foundation for Polish Science (FNP), within the scope of the WELCOME Project no. 2010-3/2.

The technical assistance of Dr. Andrzej Klepka and Lukasz Ambrozinski from the Department of Robotics and Mechatronics during the experimental tests is also greatly appreciated.

Appendix A. General solution to wave equation for a hollow cylinder

The general solution to wave equation for hollow cylinder (Eq. (1)) presented in the form of the radius-dependent f, h_r, h_θ, h_z functions involves the Bessel functions of the first J and second Y kind and is defined as

$$\begin{aligned} f(r) &= AZ_n(\alpha r)+BW_n(\alpha_1 r)\\ h_z(r) &= CZ_n(\beta_1 r)+DW_n(\beta_1 r)\\ h_r(r) &= A_1Z_{n+1}(\beta_1 r)+B_1W_{n+1}(\beta_1 r)\\ h_\theta(r) &= -A_1Z_{n+1}(\beta_1 r)-B_1W_{n+1}(\beta_1 r), \end{aligned} \tag{A.1}$$

where the constants A, B, C, D, A_1, B_1 are determined from relevant boundary conditions and the terms Z_n and W_n represent the Bessel functions J and Y or modified Bessel functions I and K of order n, and the arguments are given as $\alpha_1 r=|\alpha r|$ and $\beta_1 r=|\beta r|$. Here α, β are defined as $\alpha^2=\omega^2/v_c^2-\xi^2$ and $\beta^2=\omega^2/v_s^2-\xi^2$, for the compressional and shear bulk wave velocities denoted respectively as v_c and v_s.

The proper selection of Bessel functions in Eq. (A.1) should be made – following Table A1.

Table A1
Bessel functions of Eq. (A.1).

Interval	Functions
$\alpha^2,\ \beta^2>0$	$J_n(\alpha r)$ and $Y_n(\alpha r)$, $J_n(\beta r)$ and $Y_n(\beta r)$
$\alpha^2<0,\ \beta^2>0$	$I_n(\alpha_1 r)$ and $K_n(\alpha_1 r)$, $J_n(\beta r)$ and $Y_n(\beta r)$
$\alpha^2,\ \beta^2<0$	$I_n(\alpha r)$ and $Y_n(\alpha r)$, $I_n(\beta_1 r)$ and $K_n(\beta_1 r)$

Appendix B. Dispersion equation matrix c_{ij}

$$\begin{aligned}
c_{11} &= [2n(n-1)-(\beta^2-\xi^2)r_i^2]Z_n(\alpha_1 r_i)+2\lambda_1\alpha_1 r_i Z_{n+1}(\alpha_1 r_i),\\
c_{12} &= 2\xi\beta_1 r_i^2 Z_n(\beta_1 r_i)-2\xi r_i(n+1)Z_{n+1}(\beta_1 r_i)\\
c_{13} &= -2n(n-1)Z_n(\beta_1 r_i)+2\lambda_2 n\beta_1 r_i Z_{n+1}(\beta_1 r_i)\\
c_{14} &= [2n(n-1)-(\beta^2-\xi^2)r_i^2]W_n(\alpha_1 r_i)+2\alpha_1 aW_{n+1}(\alpha_1 r_i)\\
c_{15} &= 2\lambda_2\xi\beta_1 r_i^2 W_n(\beta_1 r_i)-2(n+1)\xi r_i W_{n+1}(\beta_1 r_i)\\
c_{16} &= -2n(n-1)W_n(\beta_1 r_i)+2n\beta_1 r_i W_{n+1}(\beta_1 r_i)\\
c_{21} &= 2n(n-1)Z_n(\alpha_1 r_i)-2\lambda_1 n\alpha_1 r_i Z_{n+1}(\alpha_1 r_i)\\
c_{22} &= -\xi\beta_1 r_i^2 Z_n(\beta_1 r_i)+2\xi r_i(n+1)Z_{n+1}(\beta_1 r_i)\\
c_{23} &= -[2n(n-1)-\beta^2 r_i^2]Z_n(\beta_1 r_i)-2\lambda_2\beta_1 r_i Z_{n+1}(\beta r_i)\\
c_{24} &= 2n(n-1)W_n(\alpha_1 r_i)-2n\alpha_1 r_i W_{n+1}(\alpha_1 r_i)\\
c_{25} &= -\lambda_2\xi\beta_1 r_i^2 W_n(\beta_1 r_i)+2\xi r_i(n+1)W_{n+1}(\beta_1 r_i)\\
c_{26} &= -[2n(n-1)-\beta^2 r_i^2]W_n(\beta_1 r_i)-2\lambda_2\beta_1 r_i W_{n+1}(\beta r_i)\\
c_{31} &= 2n\xi r_i Z_n(\alpha_1 r_i)-2\lambda_1\xi\alpha_1 r_i^2 Z_{n+1}(\alpha_1 r_i)\\
c_{32} &= n\beta_1 r_i Z_n(\beta_1 r_i)-(\beta^2-\xi^2)r_i^2 Z_{n+1}(\beta_1 r_i)\\
c_{33} &= -n\xi r_i Z_n(\beta_1 r_i)\\
c_{34} &= 2n\xi r_i W_n(\alpha_1 r_i)-2\xi\alpha_1 r_i^2 W_{n+1}(\alpha_1 r_i)\\
c_{35} &= \lambda_2 n\beta_1 r_i W_n(\beta_1 r_i)-(\beta^2-\xi^2)r_i^2 W_{n+1}(\beta_1 r_i)\\
c_{36} &= -n\xi r_i W_n(\beta_1 r_i).
\end{aligned}$$

The parameters λ_1 and λ_2 are equal to $+1$ when the Bessel functions J and Y are used and equal to -1 in the case of the modified Bessel functions I and K. Substitution of r_i by r_o in the first three rows of c_{ij} leads to the formulas for three remaining rows.

Appendix C. Asymptotic approximation of Bessel functions

Asymptotic approximation of the Bessel functions of first J and second Y kind and order n

$$J_n(x) = \sqrt{\frac{2}{\pi x}}\cos\left(x - \frac{n\pi}{2} - \frac{\pi}{4}\right) \tag{C.1}$$

$$Y_n(x) = \sqrt{\frac{2}{\pi x}}\sin\left(x - \frac{n\pi}{2} - \frac{\pi}{4}\right) \tag{C.2}$$

Appendix D. Displacements and stresses of longitudinal modes

The radial and axial displacements of axisymmetric longitudinal modes can be calculated accordingly from

$$\begin{aligned} u_r &= [f' + \xi h_r]\mathrm{e}^{\mathrm{i}(\xi z - \omega t)} \\ u_z &= \mathrm{i}[\xi f + h_r{}' + h_r/r]\mathrm{e}^{\mathrm{i}(\xi z - \omega t)}, \end{aligned} \tag{D.1}$$

and normal and tangential stresses from

$$\begin{aligned} \sigma_{rz} &= \mathrm{i}\mu(2\xi f' + (\xi^2 - \beta^2)h_r)\mathrm{e}^{\mathrm{i}(\xi z - \omega t)} \\ \sigma_{rr} &= \mu(-\lambda/\mu(\alpha^2 + \xi^2)f + 2f'' + 2\xi h_r')\mathrm{e}^{\mathrm{i}(\xi z - \omega t)}. \end{aligned} \tag{D.2}$$

Appendix E. Experimental results of three-dimensional dispersion characteristics of a thick-walled hollow cylinder

The 3-D scanning laser vibrometer was used in these tests in order to obtain the velocity responses in the X (normal), Z (axial) and Y (tangential) directions. The velocity responses were acquired with the 2.56 MHz sampling frequency. (Hollow steel cylinder with inner radius – 25 mm; thickness – 75 mm) (Figs. E1 and E2).

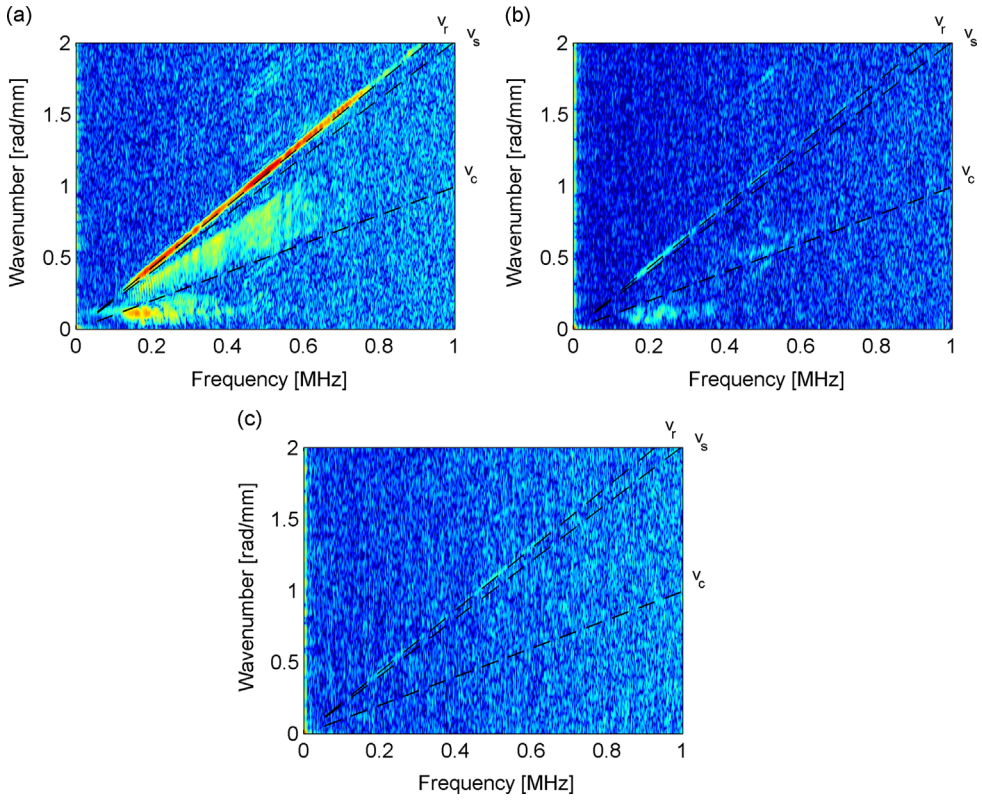

Fig. E1. Experimental wavenumber–frequency dispersion characteristics evaluated from the 3-D response data resulting from the outer surface excitation: (a) X – normal direction; (b) Z – axial direction; (c) Y – tangential direction. The dashed (– –) lines indicate the velocity limits for the guided Rayleigh wave (v_r), shear bulk wave (v_s) and compressional bulk wave (v_c).

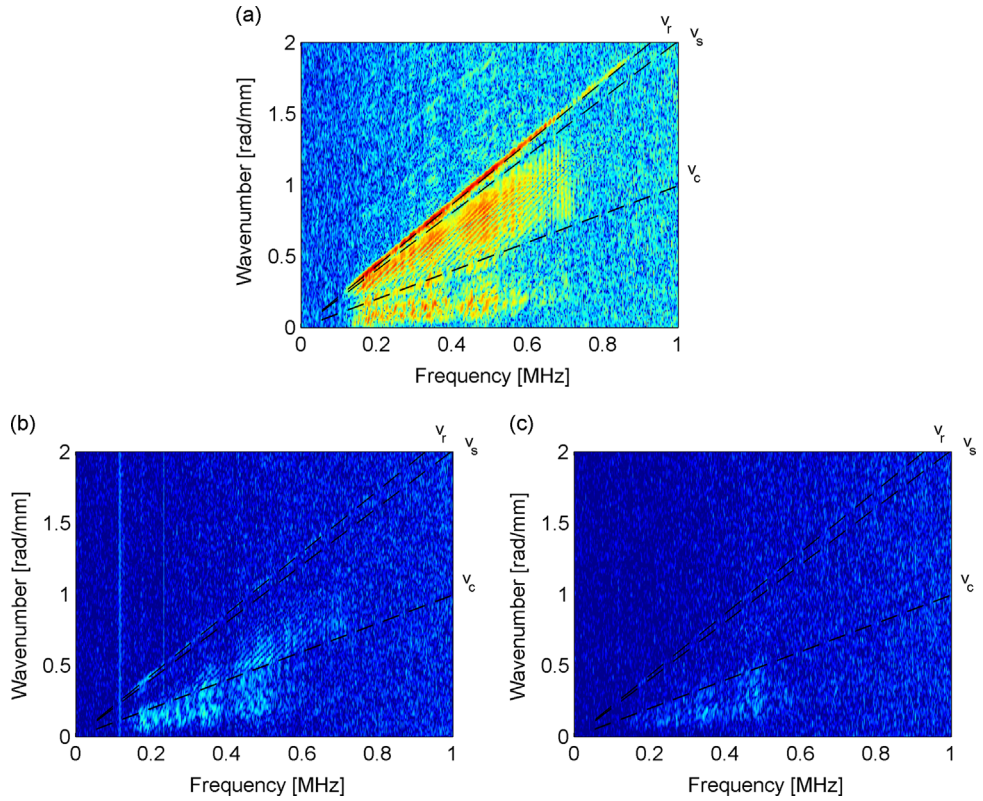

Fig. E2. Experimental wavenumber–frequency dispersion characteristics evaluated from the 3-D response data resulting from the inner surface excitation: (a) X – normal direction; (b) Z – axial direction; (c) Y – tangential direction. The dashed (– –) lines indicate the velocity limits for the guided Rayleigh wave (v_r), shear bulk wave (v_s) and compressional bulk wave (v_c).

References

[1] W. Staszewski, Structural health monitoring using guided ultrasonic waves, J. Holnicki-Szulc, C. Soares (Eds.), *Advances in Smart Technologies in Structural Engineering, Computational Methods in Applied Sciences*, Vol. 1, Springer, Berlin, Heidelberg 2004, pp. 117–162.
[2] A. Raghavan, C.E. Cesnik, Review of guided-wave structural health monitoring, *Shock and Vibration Digest* 39 (2) (2007) 91–116.
[3] S. Gopalakrishnan, M. Ruzzene, S. Hanagud, *Computational Techniques for Structural Health Monitoring*, *Springer Series in Reliability Engineering*, Springer, London, 2011, pp. 177–217.
[4] W. Staszewski, C. Boller, G.R. Tomlinson, *Health Monitoring of Aerospace Structures: Smart Sensor Technologies and Signal Processing*, John Wiley & Sons, Chichester, 2004.
[5] Z. Su, L. Ye, Y. Lu, Guided Lamb waves for identification of damage in composite structures: *a review*, *Journal of Sound and Vibration* 295 (3–5) (2006) 753–780.
[6] T. Stepinski, T. Uhl, W. Staszewski, *Advanced Structural Damage Detection: From Theory to Engineering Applications*, John Wiley & Sons, Chichester, 2013.
[7] I.A. Viktorov, *Rayleigh and Lamb Waves: Physical Theory and Applications*, Plenum Press, New York, 1970.
[8] A. Demma, P. Cawley, M. Lowe, A. Roosenbrand, B. Pavlakovic, The reflection of guided waves from notches in pipes: *a guide for interpreting corrosion measurements*, *NDT & International* 37 (2004) 167–180.
[9] R. Carandente, J. Ma, P. Cawley, The scattering of the fundamental torsional axi-symmetric defects with varying depth profile in pipes, *Journal of Acoustical Society of America* 127 (6) (2010) 3440–3448.
[10] D.C. Gazis, Three-dimensional investigation of the propagation of waves in hollow circular cylinders. I. Analytical foundation, II. Numerical results, *Journal of Acoustic Society of America* 31 (5) (1959) 568–578.
[11] M.G. Silk, K.F. Bainton, The propagation in metal tubing of ultrasonic wave modes equivalent to Lamb waves, *Ultrasonics* 17 (1) (1979) 11–19.
[12] N. Nicholson, W. McDicken, Mode propagation of ultrasound in hollow waveguides, *Ultrasonics* 29 (5) (1991) 411–416.
[13] M.J.S. Lowe, D.N. Alleyne, P. Cawley, Defect detection in pipes using guided waves, *Ultrasonics* 36 (1998) 147–154.
[14] J. Li, J.L. Rose, Natural beam focusing of non-axisymmetric guided waves in large-diameter pipes, *Ultrasonics* 44 (2006) 35–45.
[15] J.J. Ditri, J. Rose, Excitation of guided waves in hollow cylinders by applied surface tractions, *Journal of Applied Physics* 7 (1) (1992) 2589–2597.
[16] J. Li, J. Rose, Excitation and propagation of non-axisymmetric guided waves in a hollow cylinder, *Journal of Acoustical Society of America* 109 (2) (2001) 457–464.
[17] R. Carandente, P. Cawley, The effect of complex defect profiles on the reflection of the fundamental torsional mode in pipes, *NDT & International* 46 (2012) 41–47.
[18] V.K. Chillara, C.J. Lissenden, Analysis of second harmonic guided waves in pipes using a large-radius asymptotic approximation for axis-symmetric longitudinal modes, *Ultrasonics* 53 (4) (2013) 862–869.
[19] B. Hu, N. Hu, L. Li, W. Li, S. Tang, Y. Li, X. Peng, A. Homma, Y. Liu, L. Wu, H. Ning, Tomographic reconstruction of damage images in hollow cylinders using Lamb waves, *Ultrasonics* 54 (7) (2014) 2015–2023.
[20] C. Mineo, D. Cerniglia, A. Pantano, Numerical study for a new methodology of flaw detection in train axles, *Ultrasonics* 54 (3) (2014) 841–849.
[21] B. Auld, *Acoustic Fields and Waves in Solids*, Vol. II, Krieger Publishing Company, Malabar, Florida, 1973.
[22] K.F. Graff, *Wave Motion in Elastic Solids*, Dover Publications, New York, 1991.

[23] W.H. Press, S.A. Teukolsky, W.T. Vetterling, B.P. Flannery, *Numerical Recipes in C*: *The Art of Scientific Computing*, Vol. II, Cambridge University Press, Cambridge, 1973.
[24] J.A. Collins, H.R. Busby, G.H. Staab, *Mechanical Design of Machine Elements and Machines*, John Wiley & Sons, New York, 2010 (Chapter 9).
[25] A.E. Armenakas, D.C. Gazis, G. Hermann, *Free Vibrations of Circular Cylindrical Shells*, Pergamon Press, Oxford, New York, 1969.
[26] M. Ratassepp, A. Klauson, F. Chati, G. Maze, Edge resonance in semi-infinite thick pipe: *numerical predictions and measurements*, *Journal of Acoustic Society of America* 124 (2) (2008) 875–885.
[27] R.D. Mindlin, Waves and vibrations in isotropic, elastic plates, H. Deresiewicz, M. Bienek, F. DiMaggio (Eds.), *The Collected Papers of Raymond D. Mindlin, New York*, Vol. 1, 1960, pp. 425–458.
[28] L. Cheng, J. Nicolas, Free vibration analysis of a cylindrical shell-circular plate system with general coupling and various boundary conditions, *Journal of Sound and Vibration* 155 (2) (1992) 231–247.
[29] I. Tolstoy, E. Usdin, Wave propagation in elastic plates: *low and high mode dispersion*, *Journal of Acoustic Society of America* 29 (1) (1957) 37–42.
[30] M. Redwood, J. Lamb, On the propagation of high frequency compressional waves in isotropic cylinders, *Proceedings of the Physical Society* 70 (1) (1957) 136–143.
[31] A.-C. Hladky-Hennion, Finite element analysis of acoustic waves in waveguides, *Journal of Sound and Vibration* 194 (2) (1996) 119–136.
[32] I. Bartoli, A. Marzani, F.L. di Scalea, E. Viola, Modeling wave propagation in damped waveguides of arbitrary cross-section, *Journal of Sound and Vibration* 295 (3–5) (2006) 685–707.
[33] P.P. Delsanto, R.S. Schechter, H.H. Chaskelis, R.B. Mignogna, R. Kline, Connection machine simulation of ultrasonic wave propagation in materials *II. The two-dimensional case*, *Wave Motion* 20 (4) (1994) 295–314.
[34] B.C. Lee, W.J. Staszewski, Sensor location studies for damage detection with Lamb waves, *Smart Materials and Structures* 16 (2) (2007) 399–408.
[35] B.C. Lee, W.J. Staszewski, Lamb wave propagation modelling for damage detection: *I. Two-dimensional analysis*, *Smart Materials and Structures* 16 (2) (2007) 249–259.
[36] B.C. Lee, W.J. Staszewski, Lamb wave propagation modelling for damage detection: *II. Damage monitoring strategy*, *Smart Materials and Structures* 16 (2) (2007) 260–274.
[37] P. Packo, T. Bielak, A.B. Spencer, W.J. Staszewski, T. Uhl, K. Worden, Lamb wave propagation modelling and simulation using parallel processing architecture and graphical cards, *Smart Materials and Structures* 21 (7) (2012) 075001.
[38] I.A. Veres, T. Berer, C. Grünsteidl, P. Burgholzer, On the crossing points of the Lamb modes and the maxima and minima of displacements observed at the surface, *Ultrasonics* 54 (3) (2014) 759–762.